CRYSTAL GROWTH & DESIGN

ARTICLE

pubs.acs.org/crystal

Formation of Inert Bi_2Se_3(0001) Cleaved Surface

V. V. Atuchin,*[,†] V. A. Golyashov,[‡] K. A. Kokh,[§] I. V. Korolkov,[#] A. S. Kozhukhov,[⊥] V. N. Kruchinin,[∥] S. V. Makarenko,[‡] L. D. Pokrovsky,[†] I. P. Prosvirin,[○] K. N. Romanyuk,[‡] and O. E. Tereshchenko[‡,●]

[†]Laboratory of Optical Materials and Structures, Institute of Semiconductor Physics, SB RAS, Novosibirsk 630090, Russia

[‡]Department of Physics, Novosibirsk State University, Novosibirsk 630090, Russia

[§]Laboratory of Crystal Growth, Institute of Geology and Mineralogy, SB RAS, Novosibirsk 630090, Russia

[#]Laboratory of Crystal Chemistry, Institute of Inorganic Chemistry, SB RAS, Novosibirsk 630090, Russia

[⊥]Laboratory of Nanodiagnostics and Nanolithography, Institute of Semiconductor Physics, SB RAS, Novosibirsk 630090, Russia

[∥]Laboratory for Ellipsometry of Semiconductor Materials and Structures, Institute of Semiconductor Physics, SB RAS, Novosibirsk 630090, Russia

[○]Boreskov Institute of Catalysis, SB RAS, Novosibirsk 630090, Russia

[●]Laboratory of Molecular Beam Epitaxy of III-V Semiconductors, Institute of Semiconductor Physics, SB RAS, Novosibirsk 630090, Russia

Supporting Information

ABSTRACT: A high quality inclusion-free Bi_2Se_3 crystal has been grown by the Bridgman method with the use of a rotating heat field. A large-area atomically flat Bi_2Se_3(0001) surface of excellent crystallographic quality has been formed by cleavage. Chemical and microstructural properties of the surface have been evaluated with reflection high-energy electron diffraction, atomic force microscopy (AFM), scanning tunneling microscopy (STM), spectroscopic ellipsometry, and X-ray photoelectron spectroscopy. There was no Bi_2Se_3(0001) surface oxidation detected after over a month in air under ambient conditions as shown by comparative core level spectroscopy, AFM, and STM.

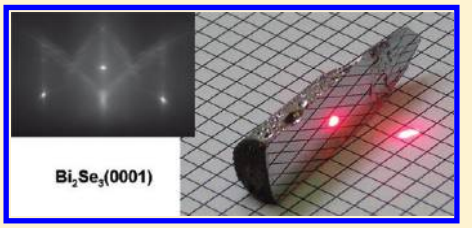

INTRODUCTION

Bismuth selenide, Bi_2Se_3, is a compound well-known for its pronounced layered crystal structure and good thermoelectric properties.[1−3] In recent years, the crystal has attracted great attention as a three-dimensional topological insulator (TI).[4−9] This new electronic system is characterized by a combination of an insulating bulk and conducting surface states of massless Dirac fermions. Several methods have been proposed for the experimental realization of such electronic states at the crystalline surface of Bi_2Se_3. Epitaxial thin films and nanocrystals can be used for an observation of the TI surface electronic effects.[6,10−14] Because of good cleavage properties of Bi_2Se_3 crystal, the (0001) surface can be prepared by mechanical cleaving of the bulk crystal, and this method was also used in several experiments on the TI effect observation but without a clear description of crystal growth conditions and surface preparation.[7,9,15−18] The formation and stability of TI state at the crystal−vacuum (or crystal −air) boundary, however, may be strongly dependent on the structural and chemical quality of Bi_2Se_3 crystal, and the top surface properties seem to be among the governing factors.

Generally, it is known that halcogenide compounds tend to oxidize in air due to their drastic affinity with oxygen.[19−24] For many complex halcogenide compounds, the chemical interaction with air agents results in complete decomposition and amorphization with time that limits the crystal living period. From this common point of view, the Bi_2Se_3 crystal appears to be not an exception, and, respectively, oxide presence could be expected at the crystal surface. Indeed, oxygen signal was detected by X-ray photoelectron spectroscopy in several studies devoted to a complex evaluation of the Bi_2Se_3 nanocrystals prepared by hydrothermal reactions.[25−27] The behavior of cleaved Bi_2Se_3(0001) surface is less clear. On the one hand, there are reports on swift oxidation of Bi_2Se_3(0001) surface in air at ambient and increased temperatures.[28,29] On the other hand, layered halcogenide crystals generally display a pronounced chemical inertness of the cleaved surface. For example, the cleaved Se-terminated optical-quality surface of GaSe crystal is long-living in air and widely applied in nonlinear optical devices.[30]

The crystal structure of trigonal Bi_2Se_3, space group $R\bar{3}m$, is shown in Figure 1.[31,32] The crystal lattice of this modification is formed by bilayers of face-sharing $BiSe_6$ octahedrons (quintuple). The bilayers are stacked along the *c* axis by weak van der Waals bonds with a Se−Se distance as long as 351 pm. On cleavage these long Se−Se bonds are disrupted, and after relaxation the

Received: August 18, 2011
Revised: October 5, 2011
Published: October 10, 2011

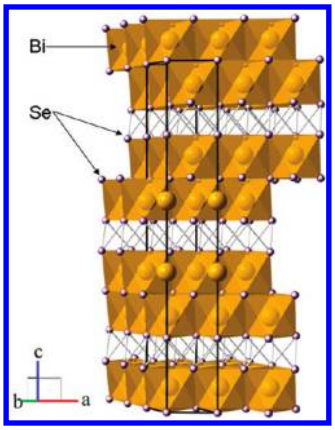

Figure 1. Crystal structure of Bi_2Se_3. Hexagonal unit cell is outlined. Lone atoms of selenium and bismuth are omitted for clarity.

(0001) surface is supposed to be Se-terminated. Respectively, the top surface chemical behavior seems to be similar to that of cleaved GaSe surface, and chemical inertness can be reasonably supposed. Additively, it should be noted that the phase transition of Bi_2Se_3 into orthorhombic modification with the structure related to Sb_2S_3 type was found at high temperature and pressure.[33] The orthorhombic modification is metastable under normal conditions. Other properties of orthorhombic Bi_2Se_3 remain unknown.

Thus, available information on the properties of cleaved Bi_2Se_3(0001) surface is a subject for serious questions. For this reason, the thin film molecular beam epitaxial technique and crystal cleavage in an ultrahigh vacuum chamber or a special glovebox with inert gas atmosphere are the techniques usually applied for the preparation of clean Bi_2Se_3 surface that greatly complicate TI sample technology.[6,7,11,14,15] The present study is aimed at a complex evaluation of microstructural and chemical properties of the Bi_2Se_3(0001) cleaved surface. For this purpose, the high-quality Bi_2Se_3 crystal was grown by the developed Bridgman technique. The cleaved crystal surface was evaluated by reflection high-energy electron diffraction (RHEED), atomic force microscopy (AFM), scanning tunneling microscope (STM), and X-ray photoelectron spectroscopy (XPS) methods as a function of time in the air atmosphere.

EXPERIMENTAL SECTION

Bi_2Se_3 melts congruently at T = 705 °C and forms eutectic in the Se-rich part of the Bi−Se system.[34] The Bi-rich part of the Bi−Se phase diagram is more complicated and consists of a sequence of peritectic reactions. Active oxidation of the Bi−Se melt in the air atmosphere requires crystal growth processing to be performed in a "closed" system, for example, in evacuated fused quartz ampule. Because of partial selenium volatilization into the ampule free volume, the stoichiometry of the melt composition becomes a problem. Therefore, Bi_2Se_3 crystallization from the melt enriched by 1 mol % of Se seems to be more convenient because the process would be reliably shifted out of peritectic reactions. A vapor pressure of the elementary components is not critical for the quartz ampule resistance. So, the compound charge may be obtained by direct alloying of elementary components.

In this work the charge prepared from elementary Bi (5N) and Se (4N) in composition $Bi_2Se_{3.01}$ was sealed into the fused quartz ampule evacuated up to ~10^{-4} Torr. High-purity bismuth was prepared in NIIC (Novosibirsk, Russia).[35] The mixture heated up to 20 °C above the melting temperature was kept for 24 h to finish the reaction between the components, and then it was cooled together with the furnace. The synthesized polycrystalline ingot was reloaded into the special quartz ampule with a conical tip for recrystallization by a modified vertical Bridgman method using the rotating heat field .[36,37] In order to prevent sticking between the growing crystal and fused quartz, the internal walls of the ampule were coated with pyrolytic carbon.[38] The ampoule translation rate and axial temperature gradient were 10 mm/day and ~15 °C/cm, respectively. As a result, a crystal 9 mm in diameter and 60 mm long was grown.

Phase compositions of both the synthesized and recrystallized Bi_2Se_3 were evaluated with X-ray diffraction (XRD) analysis. XRD patterns were recorded using Shimadzu XRD-7000 (Cu Kα radiation, Ni-filter, 5−60° 2θ range) device. A polycrystalline sample was gently ground using a hexane bath in an agate mortar, and the resulting suspension was deposited on the polished side of a standard silica sample holder to have a smooth thin layer formed after drying. Indexing of the diffraction patterns was carried out using the data for compounds reported in the PDF database [Powder Diffraction File. Alphabetical Index. Inorganic phases, JCPDS, 1983 (International Center for Diffraction Data, Pennsylvania, USA)]. The presence of pure Bi_2Se_3 phase was verified for the as-synthesized sample and the crystal grown. No indication of any foreign phase presence, including the known Bi-reached bismuth selenides and high-temperature Bi_2Se_3 II, was detected in the XRD patterns as shown in Figures 1S and 2S, Supporting Information.

The electrophysical parameters of the Bi_2Se_3 crystal were measured by the Van-der-Pau technique based on the Hall effect. A cleaved sample with the area of ~1 cm^2 and thickness of 0.5 mm was used in this experiment. The magnetic field was 19.2 kGs (1.92 T) and the current was 20 mA. The n-type of conductivity is found with the carrier concentration n = 1.4 × 10^{19} cm^{-3} and 1.3 × 10^{19} cm^{-3} and carrier mobility μ = 880 $cm^2/(V\ s)$ and 1380 $cm^2/(V\ s)$ at 293 and 77 K, respectively.

The substrates of Bi_2Se_3(0001) with dimensions up to 9 × 1 × 50 mm^3 were prepared by cleaving the crystal with a steel knife in the air atmosphere. Top-surface crystallographic properties were evaluated with RHEED using an EFZ4 device under electron energy 50 keV. RHEED observation was produced during an hour after crystal cleavage. Surface micromorphology of the substrates was studied by AFM in the noncontact mode with Solver P-47H device. AFM observation was performed by 4 and 30 days after the surface preparation.

Electronic properties of the Bi_2Se_3 surface were characterized by XPS. The XPS valence-band and core-level spectra of Bi_2Se_3 were measured using the UHV-analysis-system assembled by SPECS (Germany). The system is equipped with a PHOIBOS 150 hemispherical analyzer. A base pressure of a sublimation ion-pumped chamber of the system was less than 6 × 10^{-10} mbar during the present experiments. The Al Kα radiation (E = 1486.6 eV) was used as a source of photoelectron excitation. The XPS spectra were recorded at the constant pass energy of 10 eV. The energy scale of the spectrometer was calibrated by setting the measured Au $4f_{7/2}$ and Cu $2p_{3/2}$ binding energies (BE) to 84.00 ± 0.05 eV and 932.66 ± 0.05 eV, respectively, in reference to the Fermi energy, E_F. The energy drift due to charging effects was not detected due to noticeable bulk conductivity of the samples except for pure selenium. For the peak fitting procedure, a mixture of Lorenzian and Gaussian functions were used together with the Shirley background subtraction method.

To determine the chemical composition of the Bi_2Se_3 surface, the atomic sensitivity factors (ASF) were defined using pure polycrystalline Bi and Se samples. To remove the surface contaminations that appeared due to interaction with air, a bombardment of Bi sample surface was performed by Ar^+ ions with an energy of 1.05 keV (3−4 μA) up to exhausting the O 1s photoemission signal. To diminish the surface charging of Se surface under X-ray illumination, the measurements were produced using a powder selenium sample attached to the copper foil conductive tape. The relative element content in Bi_2Se_3 was estimated

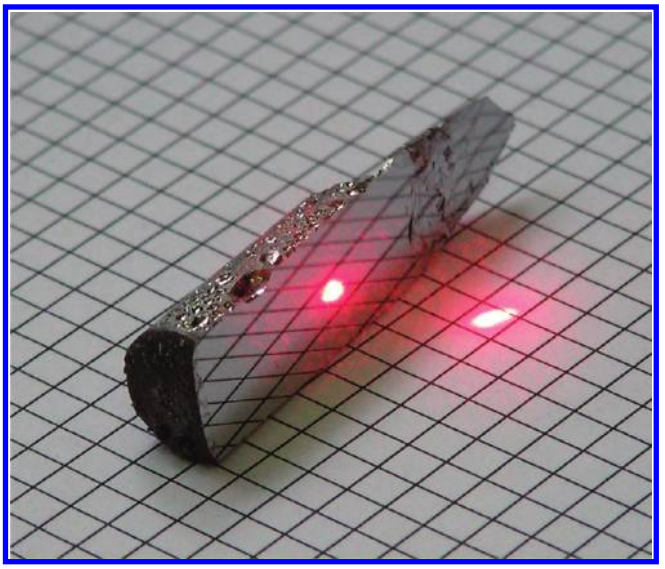

Figure 2. Cleaved Bi_2Se_3 crystal on the scale grid of 5 × 5 mm^2.

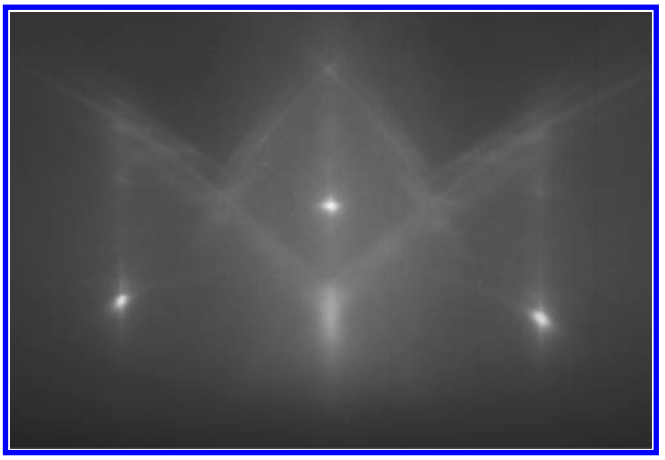

Figure 3. Kikuchi line pattern observed for Bi_2Se_3(001) surface by RHEED analysis.

by the Se $3d_{5/2}$ and Bi $4f_{7/2}$ lines recorded for the fresh cleaved Bi_2Se_3 surface. The result of calculations Se/Bi = 1.54 is in good agreement with the nominal composition Se/Bi = 1.50 of Bi_2Se_3.

The STM images and profile measurements were obtained at room temperature in a ultra high vacuum (UHV) chamber with a base pressure $\sim 1 \times 10^{-10}$ Torr with an Omicron STM for the Bi_2Se_3(0001) samples prepared by cleavage in the air atmosphere. Cleaved samples were kept in the air for two weeks before STM measurements.

Spectral dependencies of refractive index $n(\lambda)$ and extinction coefficient $k(\lambda)$ were determined by means of spectroscopic ellipsometry (SE). Ellipsometric angles Ψ and Δ were measured as a function of λ over the spectral range ~250−1030 nm using an ELLIPS-1771 SA ellipsometer.[39] The instrument spectral resolution was 2 nm, the recording time of a spectrum did not exceed 20 s, and the angle of incidence of light beam on the sample surface was 70°. We used the four-zone method of SE measurements with subsequent averaging over all the four zones. Ellipsometric parameters Ψ and Δ are related to the complex Fresnel reflection coefficients by the equation:

$$tg\Psi e^{i\Delta} = \frac{R_p}{R_s}$$

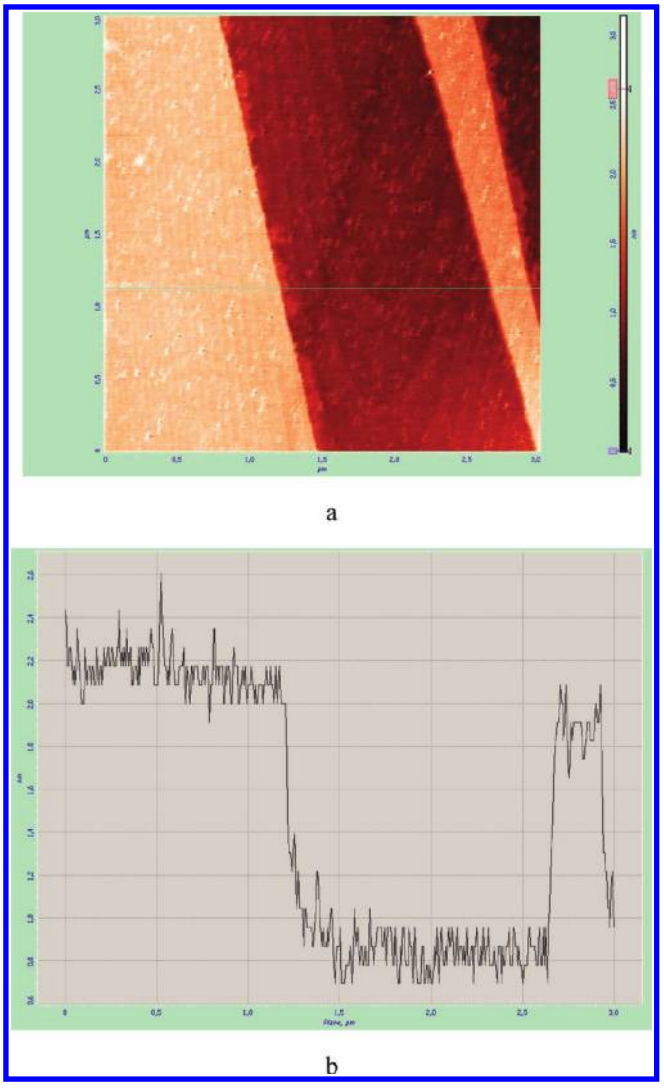

Figure 4. (a) AFM image and (b) depth profile recorded for Bi_2Se_3-(0001) surface.

where R_p and R_s are the coefficients for p and s lightwave polarizations. To calculate the dependencies of refractive index $n(\lambda)$ and extinction coefficient $k(\lambda)$, the experimental data were processed using the model of (air) − (homogeneous isotropic substrate).

RESULTS AND DISCUSSION

The fragment of as-grown crystal with a cleaved surface is shown in Figure 2. A mirror-quality surface with the area of several cm^2 is formed by cleavage that indicates a single-crystal nature of the boule bulk. Earlier, a comparatively large area of uniform cleaved surface was only demonstrated for $Bi_{1.9}Tl_{0.1}Se_3$ crystal.[40] The result of RHEED observation of cleaved Bi_2Se_3-(0001) surface is presented in Figure 3. As one can see from the figure, a perfect system of Kikuchi lines is observed for the surface. This RHEED pattern indicates a high crystallographic quality of the cleaved Bi_2Se_3(0001) surface. The 3-fold crystallographic axis normal to cleaved surface was confirmed by the sample rotation. As it was shown by AFM observation, the cleaved Bi_2Se_3(0001) surface is almost entirely atomically flat with an as low rms parameter as ~0.06 nm defined for the area of 5 × 5 μm^2. During AFM observation, it was a very difficult task to

dx.doi.org/10.1021/cg201163v |Cryst. Growth Des. 2011, 11, 5507–5514

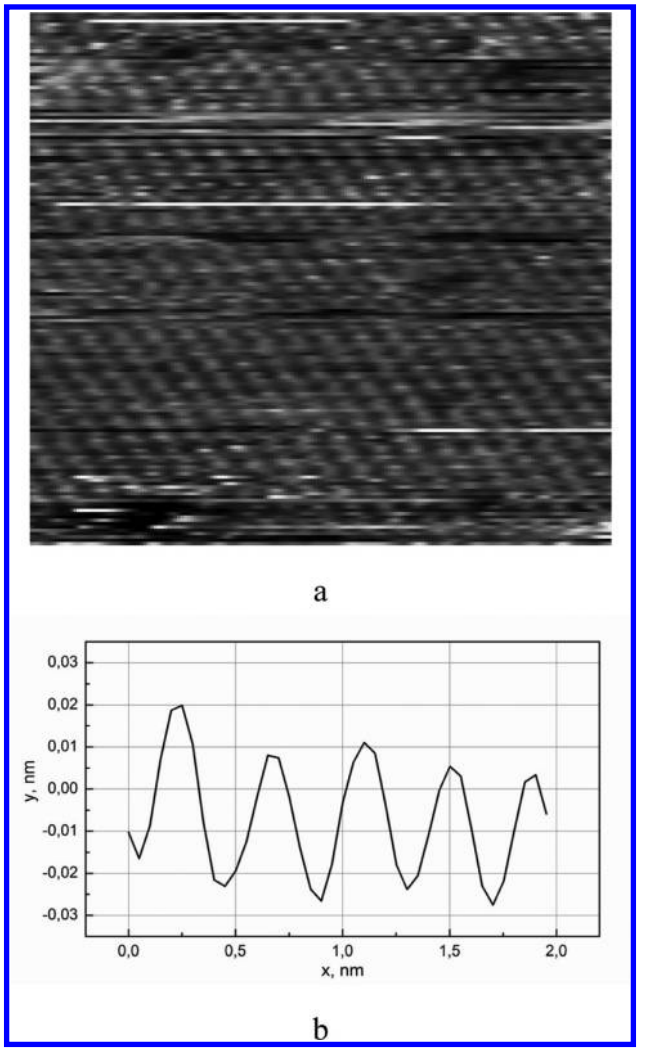

Figure 5. STM (a) 8 × 8 nm^2 topographic image of Bi_2Se_3(0001) cleaved surface acquired at a bias voltage of −0.8 V and (b) cross-sectional profile recorded after two weeks of exposure to air.

find a field with residual terraces over the sample area of ~2 cm^2. Contrary to an earlier report on the hillock-type micromorphology of cleaved Bi_2Se_3(0001) surface,[28] no such structures were observed in our experiment. An example of AFM pattern recorded for the field of 3 × 3 μm^2 with terraces is shown in Figure 4. Two parallel flat terraces with scattered mesoscale structural defects are observed for this field. The height of the elemental step of ~1.1 ± 0.1 nm is close to the value of $c/3$ of Bi_2Se_3 related to the thickness of a bilayer of $BiSe_6$ octahedrons (quintuple).[31] Earlier, the formation of crystalline Bi_2Se_3 islands or step layer on Si surface was performed by molecular beam epitaxy.[6] The height of the islands or terrace steps was estimated by STM as 0.95 nm that is in good relation with the value defined in our AFM experiment. Thus, the AFM results confirm the idea that a quintuple layer is a minimum building block at the Bi_2Se_3(0001) surface for the high quality material. The steps with lower height, however, seem to be possible for defect crystal parts.[15]

The filled state STM image shown in Figure 5a was measured in the constant current mode at a bias voltage of −0.8 V and tunneling current of 0.1 nA. The Bi_2Se_3(0001) surface is atomically clean and is presented by surface structure 1 × 1 with a

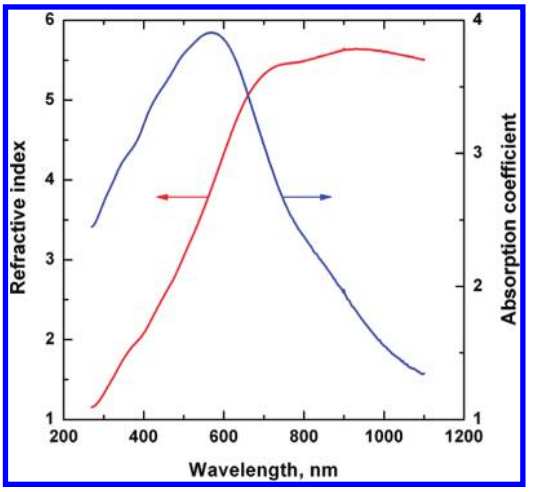

Figure 6. Dispersion of refractive index and absorption coefficient in Bi_2Se_3.

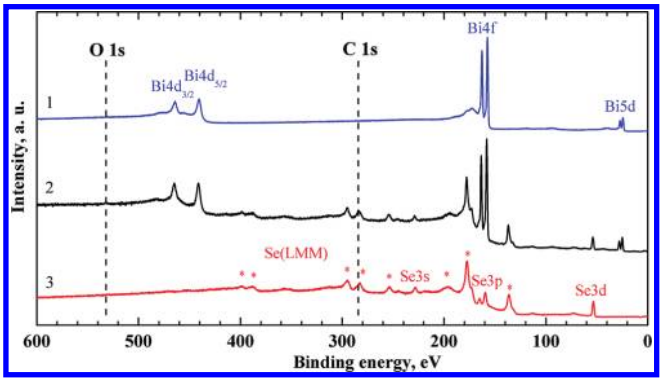

Figure 7. Survey photoelectron spectra of bombarded (1) Bi and (3) Se surfaces, and (2) Bi_2Se_3(0001) cleaved surface.

period of 0.4 nm as shown in Figure 5b. The Bi_2Se_3(0001) surface contains a low concentration of mobile adsorbed atoms (molecules) associated with horizontal lines in the STM image (Figure 5a). Because of the high diffusivity, these adsorbed atoms cannot be located in the STM images. However, because of weak bonding to the Bi_2Se_3(0001) surface, the adsorbed atoms can easily jump from the surface to a tip. Each jump induces a modification of the tip resulting in different contrast horizontal lines in the STM image. Low concentration and high diffusivity of the adsorbed atoms (molecules) at room temperature on the Bi_2Se_3(0001) surface are also associated with a pronounced chemical inertness of the surface.

Refractive index and absorption coefficient defined as a function of optical wavelength are shown in Figure 6. The curves were derived using a simple model of (air) − (homogeneous isotropic infinite substrate) without the account of an interface layer, possible surface roughness and other factors affecting ellipsometric angles. Details of the algorithm used for calculations can be found elsewhere.[41] In the framework of the model, optical parameters n and k can be calculated analytically for each wavelength. Generally, a very high refractive index is found for photon energy $E \sim 2.14$ eV. Strong absorption is observed over the energy range $E = 1.03-2.07$ eV.

A survey XPS spectrum of the cleaved Bi_2Se_3(001) surface recorded after a month of contact with the air at ambient

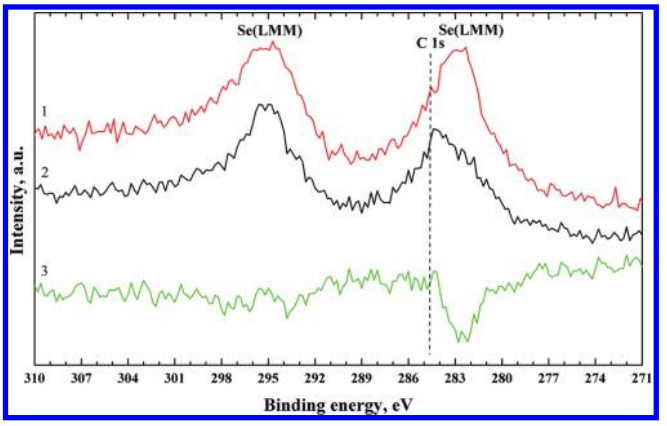

Figure 8. Detailed photoelectron spectra of C 1s window recorded for (1) elemental Se, (2) Bi_2Se_3 and (3) difference spectrum.

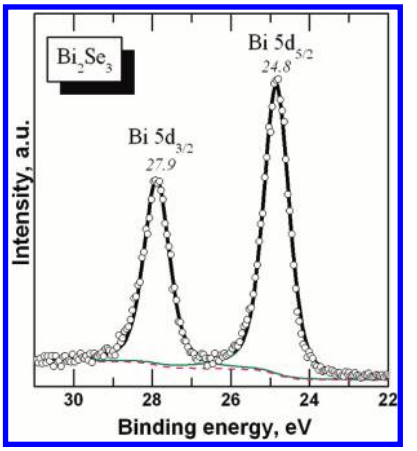

Figure 9. Detailed photoelectron spectrum of Bi 5d doublet in Bi_2Se_3.

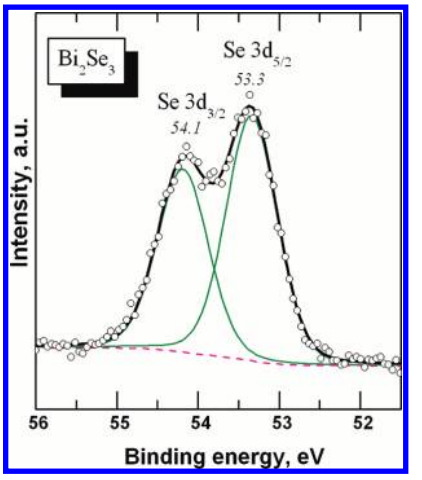

Figure 10. Detailed photoelectron spectrum of Se 3d doublet in Bi_2Se_3.

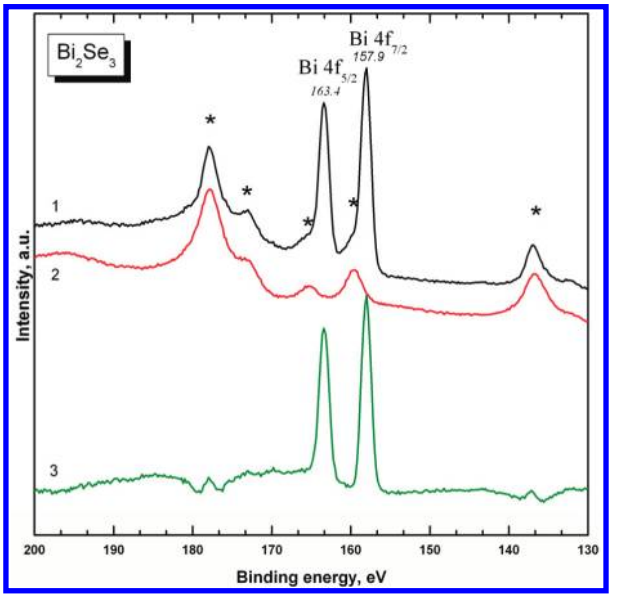

Figure 11. Detailed photoelectron spectrum of (1) Bi 4f window in Bi_2Se_3, (2) elemental Se with BE shifting, and (3) difference spectrum. Selenium lines in Bi_2Se_3 are indicated by stars.

conditions is shown in Figure 7 together with the spectra recorded for elemental Bi and Se surfaces. The photoelectron spectra of polycrystalline Bi and Se plates were recorded after the surface cleaning by ion bombardment implemented to remove native oxides. All the spectral features observed in the photoemission spectra of Bi_2Se_3, Bi, and Se were unambiguously attributed to constituent element core-levels and a suite of selenium Auger lines. As it may be supposed, long time contact with the air results in partial oxidation of the $Bi_2Se_3(0001)$ surface similar to other selenides.[19,20,22] However, there is no detectable O 1s signal from the as-inserted $Bi_2Se_3(0001)$ surface. This faithfully indicates high chemical inertness of the cleaved Bi_2Se_3 surface in reference to oxidation in the air under ambient conditions. The result is in evident contradiction with the swift oxidation kinetics found by XPS for the cleaved $Bi_2Se_3(0001)$ surface in ref 29.

It is interesting to evaluate the intensity of hydrocarbon adsorption from the air at the cleaved $Bi_2Se_3(0001)$ surface because this air agent is the most typical surface contamination. The C 1s window is shown in Figure 8. In Se-bearing compounds the characteristic C 1s line, typically observed at BE of 284−285 eV, is superposed with an intensive selenium Auger line with a maximum at ∼283 eV. The hydrocarbons are absent at the Se surface used as reference because the adsorbed species were removed by ion bombardment. To reveal the C 1s signal at the Bi_2Se_3 surface, the difference spectrum was obtained by subtraction of the spectrum of bombarded Se surface from that recorded for $Bi_2Se_3(0001)$ with relative intensity calibration made for the selenium Auger line at ∼295 eV. From observation of the difference spectrum, the absence of a noticeable C 1s signal over the BE range of 284−285 eV at the Bi_2Se_3 surface is obvious. This indicates high inertness of the $Bi_2Se_3(0001)$ cleaved surface in reference to hydrocarbon adsorption from the air environment.

The detailed photoelectron spectra of Bi 5d, Se 3d, and Bi 4f doublets recorded for $Bi_2Se_3(0001)$ surface after a month exposure in the air are shown in Figures 9−11. The Bi 5d and Se 3d doublets can be well approximated by a combination of individual components that verify unique chemical states of bismuth and selenium in Bi_2Se_3. The Bi 4f doublet shown in Figure 11 is somewhat distorted, as it appears due to the superposition with a low intensity Se 3p doublet. To estimate the effect of the superposition on the BE(Bi $4f_{7/2}$), subtraction of elemental selenium spectrum from the Bi_2Se_3 spectrum was

dx.doi.org/10.1021/cg201163v |Cryst. Growth Des. 2011, 11, 5507–5514

Table 1. Binding Energies of Constituent Element Core Levels of Bi_2Se_3

form	Bi $5d_{5/2}$	Se $3d_{5/2}$	Bi $4f_{7/2}$	foreign lines	ref
crystal, cleaved	24.6	53.5, 54.2	157.7	C 1s, O 1s	42
crystal, cleaved	24.55	52.95		?[b]	43
film, amorphous	25.1	54.1[a]		?[b]	44
film, crystalline	25.0	53.7[a]		?[b]	44
crystal, cleaved	24.8	53.7[a]	157.9		45
crystal, sputtered	24.5	53.3	157.6		46
nano		~52.9[a]	157.4	C 1s, O 1s	25
nano		~53.4[a]	158.0	C 1s, O 1s	26
nano		~51.7[a]	156.0	C 1s, O 1s	27
film		53.7	158.1		47
crystal, cleaved	24.8	53.35	157.9		this study
scattering range, eV	0.6	2.5	2.1		

[a] Se 3d doublet is not resolved. [b] No information reported.

Table 2. Binding Energies of Constituent Element Core Levels of Elemental Bi and Se

core level, eV	Bi $5d_{5/2}$	Se $3d_{5/2}$	Bi $4f_{7/2}$	ref
Bi	23.5		156.6	46
			157.0	56
	26.9		156.9	58
	27.0		157.0	54
	24.2			42
	24.8		157.3	this study
Se		54.5		46
		55.0[a]		59
		55.6		57
		55.5[a]		42
		55.5[a]		60
		55.7		this study

[a] Se 3d doublet is not resolved.

implemented by accounting relative intensity and BE scale linkage produced for the selenium Auger line at ~177 eV.

The resulting difference spectrum shows no noticeable BE energy shift of Bi 4f doublet. Thus, the BE(Bi $4f_{7/2}$) obtained from the Bi_2Se_3 spectrum can be used as a representative parameter related to the bismuth chemical state in this selenide.

A set of BE values of representative core levels measured for Bi_2Se_3 is summarized in Table 1 together with the parameters reported in the literature for different Bi_2Se_3 forms. Giant scattering in BE values available for this compound is evident. The ranges are as high as 0.6, 2.5, and 2.1 eV for Bi$5d_{5/2}$, Se $3d_{5/2}$, and Bi $4f_{7/2}$ lines, respectively. Several factors, as it appears, define the scattering of the above-mentioned BE values, and the difference in the BE scale calibration method seems to be most significant. Besides, in several studies the Se 3d doublet was not resolved and that results in overestimated BE (Se $3d_{5/2}$) values. In addition, the Bi_2Se_3 nanocrystals synthesized by a chemical route could have surface contaminations with reagent residuals. To reduce the significance of these hard-to-control factors, it is suitable to use the BE difference, Δ_1 = BE (Se $3d_{5/2}$) − BE (Bi $5d_{5/2}$) or Δ_2 = BE (Bi $4f_{7/2}$) − BE (Se $3d_{5/2}$), as a key characteristic parameter instead of the BE of a representative photoelectron line. Previously, a higher robustness of BE difference parameters was demonstrated for various oxides, sulfide and bromide compounds.[23,24,48−53] This algorithm can be successfully applied for the parameters shown in Table 1 by decreasing the scatter range to 0.45 and 0.4 eV for Δ_1 and Δ_2. From our experiment, the values of BE difference parameters for Bi_2Se_3(0001) are equal to Δ_1 = 28.55 and Δ_2 = 104.55 eV.

Detailed photoelectron spectra of Se 3d and Bi 4f doublets recorded for a clean surface of elemental Se and Bi are shown in Figures 3S and 4S, Supporting Information. As it may be assumed, the top surface of selenium and bismuth samples is amorphous after ion bombardment. Nevertheless, doublets are well resolved and can be approximated by a combination of individual components. In Se-bearing oxides the energy position of Se 3d doublet is drastically shifted to higher BE values and typically observed at ~60 eV.[54,55] Such a line is completely absent in the spectrum shown in Figure 3S, Supporting Information that confirms pure metal selenium state after ion bombardment. As to bismuth oxides, the Bi $4f_{7/2}$ line related to Bi−O bonds is appeared at BE ~ 159.5−160 eV.[54,56,57] A weak signal is found in this spectral range in Figure 4S, Supporting Information. The BE values defined for elemental Se and Bi are shown in Table 2 together with the earlier results. Great scattering is observed in the parameters, as it seems due to the difference in BE scale calibration and surface preparation.

The parameter Δ_2 calculated for elemental Se and Bi is equal to 101.6 eV. On Bi−Se chemical bond formation in Bi_2Se_3, the valence electron transfer occurs from Bi to Se atoms. The effective displacement of valence electron density away from atomic nucleus results in the reduction of electrical screening of inner shells with an increase of binding energies for inner electrons. So, when the Bi−Se bond forms, the electron density transfer induces a shift of Bi $4f_{7/2}$ level to higher BE and a shift of Se $3d_{5/2}$ to lower BE in reference to BE values of elemental Bi and Se. The variation of Δ_2 parameter achieves ~3 eV and is induced dominantly by BE(Se $3d_{5/2}$) variation. So, the values of Δ_i are very sensitive to chemical effects and can be used as a suitable parameter for Bi−Se bonding characterization.

Outstanding chemical stability of cleaved Bi_2Se_3(0001) surface obtained in our experiment is in good relation with the general tendency known for many selenide crystals with layered structure. Low chemical reactivity in the air environment was earlier demonstrated for GaSe, InSe, In_4Se_3, $TlGaSe_2$, and other layered selenides when the crystal surface was prepared by cleavage or special treatments to have a high surface structural quality.[22,61−65] Most interesting examples are the InSe and GaSe crystals where atomic layers are linked by weak van der Waals bonds similar with that of Bi_2Se_3 and the Se-terminated optical surface can be formed by cleavage.[38,61,62,66−68] Cleaved (001) surface of InSe or GaSe is atomically flat and characterized by a very long living period in the air due to the absence of selenium dangling bonds. Respectively, for these crystals, the surface oxidation was detectable only after several months under ambient conditions.[61,62,69,70] Surface oxidation of GaSe(001) starts by gallium oxide formation and appears to be controlled by defects at a cleaved surface.[69,70] We know from our own laboratory practice in GaSe nonlinear optical element handling that the low-defect GaSe crystals grown under an applied rotating heat field give a very stable cleaved surface. The recently reported rapid oxidation of Bi_2Se_3(0001) surface during 2−5 days was found to be initiated by bismuth oxidation.[29] This result is in evident

contradiction with our measurements for $Bi_2Se_3(0001)$ cleaved surface of a high crystallographic quality. The Bi_2Se_3 crystal evaluated in ref 29 was grown by a slow cooling method when an insufficient melt mixing may be supposed. This can generate defects in the selenium shield at the cleaved surface with an access appearing for oxygen to underlying bismuth atoms that results in the enforcement of the surface oxidation process. Comparatively, the low defect $Bi_2Se_3(0001)$ cleaved surface with a chemically inert selenium cover shows a great stability in the air at normal conditions.

CONCLUSIONS

To sum it up, we provided a comprehensive observation of microstructure, electronic parameters, and chemical activity of $Bi_2Se_3(0001)$ surface prepared by crystal cleavage. Giant area atomically flat plates of Bi_2Se_3 suitable for TI effect evaluation can be fabricated by this simple method. The cleaved surface demonstrates high chemical inertness in the air environment. There is no surface contamination or oxidation detected during a month of keeping in the air under ambient conditions. As it appears, such a pronounced surface passivation is achieved by the low-defect top layer of selenium atoms terminating a cleaved $Bi_2Se_3(0001)$ surface. Fabrication of a stable cleaved surface is possible for Bi_2Se_3 crystal grown under a rotating heat field that seems to be a key factor for homogeneous low-defect crystal formation. Evidently, the existence of a chemically stable crystal surface greatly simplifies the handling of $Bi_2Se_3(0001)$ sample in TI experiments and future device technologies.

ASSOCIATED CONTENT

Supporting Information. XRD patterns recorded for synthesized polycrystalline Bi_2Se_3 and Bi_2Se_3 crystal grown. Detailed photoelectron spectrum of Se 3d doublet for elemental Se. Detailed photoelectron spectrum of Bi 4f doublet for elemental Bi. This material is available free of charge via the Internet at http://pubs.acs.org.

AUTHOR INFORMATION

Corresponding Author

*Phone: +7 (383) 3308889. Fax: +7 (383) 3332771. E-mail: atuchin@thermo.isp.nsc.ru.

REFERENCES

(1) Vineis, C. J.; Shakouri, A.; Majaumdar, A.; Kanatzidis, M. G. *Adv. Mater.* **2010**, *22*, 3970–3980.
(2) Vaqueiro, P.; Powell, A. V. *J. Mater. Chem.* **2010**, *20*, 9577–9584.
(3) Goltzman, B. M.; Kudinov, V. A.; Smirnov, I. A. *Semiconductor Thermoelectric Materials on the Basis of Bi_2Te_3*; Nauka: Moscow, 1972.
(4) Xia, Y.; Qian, D.; Hsieh, D.; Wray, L.; Pal, A.; Lin, H.; Bansil, A.; Grauer, D.; Hor, Y. S.; Cava, R. J.; Hasan, M. Z. *Nat. Phys.* **2009**, *5*, 398–402.
(5) Zhang, H.; Liu, C.-X.; Qi, X.-L.; Dai, X.; Fang, Z.; Zhang, S.-C. *Nature Phys.* **2009**, *5*, 438–442.
(6) Cheng, P.; Song, C.; Zhang, T.; Zhang, Y.; Wang, Y.; Jia, J.-F.; Wang, J.; Wang, Yayu; Zhu, B.-F.; Chen, X.; et al. *Phys. Rev. Lett.* **2010**, *105*, 076801.
(7) Kuroda, K.; Arita, M.; Miyamoto, K.; Ye, M.; Jiang, J.; Kimura, A.; Krasovskii, E. E.; Chulkov, E. V.; Iwasawa, H.; Okuda, T.; et al. *Phys. Rev. Lett.* **2010**, *105*, 076802.
(8) Song, J.-H.; Jin, H.; Freeman, A. J. *Phys. Rev. Lett.* **2010**, *105*, 096403.
(9) Hsieh, D.; McIver, J. W.; Torchinsky, D. H.; Gardner, D. R.; Lee, Y. S.; Gedik, N. *Phys. Rev. Lett.* **2011**, *106*, 057401.
(10) Kong, D.; Dang, W.; Cha, J. J.; Li, H.; Meister, S.; Peng, H.; Liu, Z.; Cui, Y. *Nano Lett.* **2010**, *10*, 2245–2250.
(11) Zhang, Yi; Chang, C.-Z.; He, K.; Wang, L.-L.; Chen, X.; Jia, J.-F.; Ma, X.-C.; Xue, Q.-K. *Appl. Phys. Lett.* **2010**, *97*, 194102.
(12) Hong, S. S.; Kundhikanjana, W.; Cha, J. J.; Lai, K.; Kong, D.; Meister, S.; Kelly, M. A.; Shen, Z.-X.; Cui, Y. *Nano Lett.* **2010**, *10*, 3118–3122.
(13) Jin, H.; Song, J.-H.; Freeman, A. J. *Phys. Rev. B* **2011**, *83*, 125319.
(14) Chen, X.; Ma, X.-C.; He, K.; Jia, J.-F.; Xue, Q.-K. *Adv. Mater.* **2011**, *23*, 1162–1165.
(15) Urazhdin, S.; Bilc, D.; Mahanti, S. D.; Tessmer, S. H.; Kyratsi, T.; Kanatzidis, M. G. *Phys. Rev. B* **2004**, *69*, 085313.
(16) LaForge, A. D.; Frenzel, A.; Pursley, B. C.; Lin, T.; Liu, X.; Shi, J.; Basov, D. N. *Phys. Rev. B* **2010**, *81*, 125120.
(17) Sushkov, A. B.; Jenkins, G. S.; Schmadel, D. C.; Butch, N. P.; Paglione, J.; Drew, H. D. *Phys. Rev. B* **2010**, *82*, 125110.
(18) Kordyuk, A. A.; Kim, T. K.; Zabolotnyy, V. B.; Evtushinsky, D. V.; Bauch, M.; Hess, C.; Büchner, B.; Berger, H.; Borisenko, S. V. *Phys. Rev. B* **2011**, *83*, 081303(R).
(19) Lyahovitskaya, V.; Feldman, Y.; Gartsman, K.; Cohen, H.; Cytermann, C.; Cahen, D. *J. Appl. Phys.* **2002**, *91*, 4205–4212.
(20) Ihanus, J.; Lambers, E.; Holloway, P. H.; Ritala, M.; Leskelä, M. *J. Cryst. Growth* **2004**, *260*, 440–446.
(21) Yashina, L. V.; Tikhonov, E. V.; Neudachina, V. S.; Zyubina, T. S.; Chaika, A. N.; Shtanov, V. I.; Kobeleva, S. P.; Dobrovolsky, Yu. A. *Surf. Interface Anal.* **2004**, *36*, 993–996.
(22) Yablonskikh, M. V.; Berger, R.; Gelius, U.; Lizárraga, R.; Charikova, T. B.; Kurmaev, E. Z.; Moewes, A. *J. Phys.: Condens. Matter* **2006**, *18*, 1757–1768.
(23) Atuchin, V. V.; Kesler, V. G.; Parasyuk, O. V. *Surf. Rev. Lett.* **2007**, *14*, 403–409.
(24) Atuchin, V. V.; Isaenko, L. I.; Kesler, V. G.; Lobanov, S. I. *J. Alloys Comp.* **2010**, *497*, 244–248.
(25) Wang, D.; Yu, D.; Mo, M.; Liu, X.; Qian, Y. *J. Cryst. Growth* **2003**, *253*, 445–451.
(26) Yang, X.; Wang, X.; Zhang, Z. *J. Cryst. Growth* **2005**, *276*, 566–570.
(27) Ota, J. R.; Roy, P.; Srivastava, S. K.; Popovitz-Biro, R.; Tenne, R. *Nanotechnology* **2006**, *17*, 1700–1705.
(28) Ivanov, V. I.; Katerynchuk, V. M.; Kaminskii, V. M.; Kovalyuk, Z. D.; Lytvyn, O. S.; Mintyanskii, I. V. *Inorg. Mater.* **2010**, *46*, 1296–1298.
(29) Kong, D.; Cha, J. J.; Lai, K.; Peng, H.; Analytis, J.; G. Meister, S. G.; Chen, Y.; Zhang, H.-J.; Fisher, I. R.; Shen, Z.-X.; Cui, Y. *ACS Nano* **2011**, *5*, 4698–4703.
(30) Singh, N. B.; Suhre, D. R.; Bakakrishna, V.; Marable, M.; Meyer, R.; Fernelius, N.; Hopkins, F. K.; Zelmon, D. *Prog. Cryst. Growth Charact. Mater.* **1998**, *37*, 47–102.
(31) Nakajima, S. *J. Phys. Chem. Solids* **1963**, *24*, 479–485.
(32) Ozawa, T. C.; Kang, S. J. *J. Appl. Crystallogr.* **2004**, *37*, 679.
(33) Atabaeva, E. Ya.; Mashkov, S. A.; Popova, S. V. *Crystallografiya* **1973**, *18*, 173–174.
(34) Okamoto, H. *J. Phase Equilib.* **1994**, *15*, 195–201.
(35) Shevtsov, Yu. V.; Beizel, N. F. *Inorg. Mater.* **2011**, *47*, 139–142.
(36) Kokh, K. A.; Nenashev, B. G.; Kokh, A. E.; Shvedenkov, G. Yu. *J. Cryst. Growth* **2005**, *275*, e2129–e2134.
(37) Kokh, K. A.; Popov, V. N.; Kokh, A. E.; Krasin, B. A.; Nepomnyaschikh, A. I. *J. Cryst. Growth* **2007**, *303*, 253–257.
(38) Kokh, K. A.; Andreev, Yu. M.; Svetlichnyi, V. A.; Lanskii, G. V.; Kokh, A. E. *Cryst. Res. Technol.* **2011**, *46*, 327–330.
(39) Rykhlitski, S. V.; Spesivtsev, E. V.; Shvets, V. A.; Prokopiev, V. Yu. *Instrum. Experim. Techniques* **2007**, *2*, 160–161in Russian.
(40) Janček, P.; Drašar, Č.; Beneš, L.; Lošťák, P. *Cryst. Res. Technol.* **2009**, *44*, 505–510.
(41) Barton, D.; Urban, F. K., III *Thin Solid Films* **2007**, *516*, 119–127.
(42) Debies, T. P.; Rabalais, J. W. *Chem. Phys.* **1977**, *20*, 277–283.
(43) Thuler, M. R.; Benbow, R. L.; Hurych, Z. *Chem. Phys.* **1982**, *71*, 265–270.

(44) Takahashi, T.; Sagawa, T.; Hamanaka, H. *J. Non-Cryst. Solids* **1984**, *65*, 261–267.
(45) Bastl, Z.; Spirovová, I.; Janovská, M. *Coll. Czec. Chem. Commun.* **1997**, *62*, 199–212.
(46) Nascimento, V. B.; de Carvalho, V. E.; Paniago, R.; Soares, E. A.; Ladeira, L. O.; Pfannes, H. D. *J. Electron Spectrosc. Relat. Phenom.* **1999**, *104*, 99–107.
(47) Zhang, G.; Qin, H.; Teng, J.; Guo, J.; Guo, Q.; Dai, X.; Fang, Z.; Wu, K. *Appl. Phys. Lett.* **2009**, *95*, 053114.
(48) Atuchin, V. V.; Kalabin, I. E.; Kesler, V. G.; Pervukhina, N. V. *J. Electron Spectrosc. Relat. Phenom.* **2005**, *142*, 129–134.
(49) Atuchin, V. V.; Kesler, V. G.; Pervukhina, N. V.; Zhang, Z. *J. Electron Spectrosc. Relat. Phenom.* **2006**, *152*, 18–24.
(50) Atuchin, V. V.; Kesler, V. G.; Pervukhina, N. V. *Surf. Rev. Lett.* **2008**, *15*, 391–399.
(51) Atuchin, V. V.; Grivel, J.-C.; Korotkov, A. S.; Zhang, Z. *J. Solid State Chem.* **2008**, *181*, 1285–1291.
(52) Atuchin, V. V.; Isaenko, L. I.; Kesler, V. G.; Tarasova, A. Yu. *J. Cryst. Growth* **2011**, *318*, 1000–1004.
(53) Atuchin, V. V.; Galashov, E. N.; Khyzhun, O. Yu.; Kozhukhov, A. S.; Pokrovsky, L. D.; Shlegel, V. N. *Cryst. Growth Des.* **2011**, *11*, 2479–2484.
(54) Moulder, J. F.; Stickle, W. F.; Sobol, P. E.; Bomben, K. D. *Handbook of X-ray Photoelectron Spectroscopy*; Chastain, J., Ed.; Perkin-Elmer Corp.: Eden Prairie, Minnesota, 1992.
(55) Masson, D. P.; Lockwood, D. J.; Graham, M. J. *J. Appl. Phys.* **1997**, *82*, 1632–1639.
(56) Oku, M.; Kimura, J.; Omori, M.; Hirokawa, K. *Fresenius Z. Anal. Chem.* **1989**, *335*, 382–385.
(57) Walsh, A.; Watson, G. W.; Payne, D. J.; Edgell, R. G.; Guo, J.; Glans, P.-A.; Learmonth, T.; Smith, K. E. *Phys. Rev. B* **2006**, *73*, 235104.
(58) Kowalczyk, P. J.; Mahapatra, O.; McCarthy, D. N.; Kozlowski, W.; Klusek, Z.; Brown, S. A. *Surf. Sci.* **2011**, *605*, 659–667.
(59) Guo, F. Q.; Lu, K. *Phys. Rev. B* **1998**, *57*, 10414–10420.
(60) Bastl, Z.; Spirovová, I.; Horák, J. *Solid State Ionics* **1997**, *95*, 315–321.
(61) Iwakuro, H.; Tatsuyama, C.; Ichimura, S. *Jpn. J. Appl. Phys.* **1982**, *21*, 94–99.
(62) Miyake, I.; Tanpo, T.; Tatsuyama, C. *Jpn. J. Appl. Phys.* **1984**, *23*, 172–178.
(63) Galiy, P. V.; Nenchuk, T. M.; Stakhira, J. M. *J. Phys. D: Appl. Phys.* **2001**, *34*, 18–24.
(64) Neumann, H.; Yakushev, M. V.; Tomlinson, R. D. *Cryst. Res. Technol.* **2003**, *38*, 676–683.
(65) Hunger, R.; Schulmeyer, T.; Klein, A.; Jaegermann, W.; Sakurai, K.; Yamada, A.; Fons, P.; Matsubara, K.; Niki, S. *Surf. Sci.* **2004**, *557*, 263–268.
(66) Andreev, Yu. M.; Atuchin, V. V.; Lanskii, G. V.; Morozov, A. N.; Pokrovsky, L. D.; Sarkisov, S. Yu.; Voevodina, O. V. *Mater. Sci. Eng., B* **2006**, *128*, 205–210.
(67) Feng, Z.-S.; Kang, Z.-H.; Wu, F.-G.; Gao, J.-Y.; Jiang, Y.; Zhang, H.-Z.; Andreev, Yu. M.; Lanskii, G. V.; Atuchin, V. V.; Gavrilova, T. A. *Opt. Express* **2008**, *16*, 9978–9985.
(68) Sarkisov, S. Yu.; Atuchin, V. V.; Gavrilova, T. A.; Kruchinin, V. N.; Bareznaya, S. A.; Korotchenko, Z. V.; Tolbanov, O. P.; Chernyshev, A. I. *Russ. Phys. J.* **2010**, *53*, 346–352.
(69) Márquez, F.; Segura, A.; Munoz, V.; González, G. *Surf. Interface Anal.* **2002**, *34*, 460–463.
(70) Drapak, S. I.; Gavrylyuk, S. V.; Kovalyuk, Z. D.; Lytvyn, O. S. *Appl. Surf. Sci.* **2008**, *254*, 2067–2071.